NUCLEAR SCIENCE AND TECHNIQUES **25**, 040601 (2014)

The flow characteristics of fluid in micro-channels of different shapes*

WU Ge-Ping (吴鸽平),[1,†] WANG Jun (王俊),[1] and LU Ping (陆平)[1]

[1] *School of Energy and Power Engineering, Jiangsu University, Zhenjiang 212013, China*

(Received October 22, 2013; accepted in revised form December 17, 2013; published online July 7, 2014)

In this paper, we study hydrodynamics and thermal behaviors of micro-heat exchanger of different cross sections, with hydraulic diameters (D_h) of 0.4–0.8 mm and Reynolds numbers (Re) of 300–900. Validity of the model is proved by comparing simulation results based on classical Navier-Stokes equations with experimental data and Tuckerman correlation. Effects of dynamic viscosity, hydraulic diameter, Reynolds number and cross section of the micro-channels are investigated. The results indicate that the variable viscosity effect should be taken into account, and rod bundle micro-channels have the highest heat transfer coefficient of the three types of micro-channels.

Keywords: Non-uniform heating, Variable viscosity effect, Po number, Thermal efficiency

DOI: 10.13538/j.1001-8042/nst.25.040601

I. INTRODUCTION

Compact heat exchangers based on micro-channels show a nice foreground over miniature nuclear power system, and learning flow behaviors of fluid in micro-channels is of importance for designing micro-fluidic systems.

Investigations [1–5] have been devoted to flow characteristics of water in micro-channels. Koo and Kleinstreuer [6] studied viscous dissipation effects on convection through circular and rectangular micro-channels and concluded that viscous heating was a function of the hydraulic diameter, the channel aspect ratio, and the Brinkman number, and that ignoring viscous dissipation could affect accurate flow simulation in micro-channels.

Judy *et al*. [7] experimented with distilled water, methanol, and isopropanol in round and square micro-channels fabricated from fused silica and stainless steel, and measured frictional pressure drop in hydraulic diameters of $D_h = 15$–$150\,\mu m$ over Reynolds number of $Re = 8$–2300. The results showed that the values of fRe agreed well with the conventional Stokes flow theory over the tested range of Reynolds numbers.

Gamrat *et al*. [8] performed both two- and three-dimensional numerical simulation to analyze thermal entrance effects on micro-channel convection. They found that the continuum model of conventional mass, Navier–Stokes and energy equations were adequately accurate to simulate the fluid flow and heat transfer for the micro-channels.

Against researches in the past decade in a micro-channel of single shape, however, there is just a handful of studies, experimental or theoretical, on flow characteristics of micro-channels in different shapes. In this paper, we study hydrodynamic and thermal behavior of fluid flow in micro-channel heat exchanger of different shapes. The effects of dynamic viscosity, hydraulic diameter, Reynolds number and cross sections are investigated.

II. EXPERIMENTAL SETUP

The experimental system used in this study is divided into three parts–the test section, the water driving system, and the dynamic data acquisition section, as shown schematically in Fig. 1.

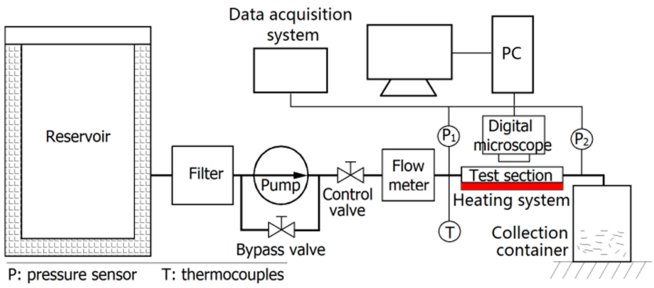

Fig. 1. (Color online) Schematic of the experimental system.

Effective hermetically sealing and heat insulating measures were taken for the test section. Fluid flow through the test section could be adjusted by the control valve. Deionized water was used as the working fluid. A flow meter was connected at the entrance of the test section. Two pressure sensors were fixed on the inlet and outlet ducts to measure pressure. Type-K thermocouples were selected to measure temperatures of solid wall and liquid. Heating pillars powered by a DC power supply, which can be regulated, were used to supply constant heat flux. The measurement signals were transmitted to a computer.

The physical configurations of the micro-channels heat exchanger are shown schematically in Fig. 2. The dimensions of cooling passages are given in Table 1.

* Supported by National Natural Science Foundation of China (No. 51106067), China Postdoctoral Science Foundation (No. 2012M511212) and Foundation of Priority Academic Program Development of Jiangsu Higher Education Institutions

† Corresponding author, gpwu@mail.ujs.edu.cn

TABLE 1. Dimensions of the micro-channels (μm)

D_h	H	W_1	R_1	R_2	W_2	W_c	L
400	2200	220	200	210	140	20	10000
600	3300	330	300	300	200	20	10000
800	4400	440	400	420	280	20	10000

III. MATHEMATICAL MODEL

According to the literature, Navier-Stokes equations are still valid for laminar flow of water in micro-channels of hydraulic diameter as small as 0.4 mm. The model is derived from continuum based on conservation equations of mass, momentum and energy, with the following basic assumptions: (1) negligible effect of gravity and other forms of body forces, (2) incompressible Newtonian fluid, and (3) steady laminar flow.

The governing equations are Eqs. (1)– (3), the equations of continuity, momentum and energy, respectively.

$$\nabla\vec{V} = 0, \tag{1}$$

$$\rho_f(\vec{V}\cdot\nabla\vec{V}) = -\nabla p + \mu_f\nabla^2\vec{V} + S_\mu\nabla T\cdot def\vec{V}, \tag{2}$$

$$\rho_f c_{p,f}(\vec{V}\cdot\nabla T) = k_f\nabla^2 T + \phi, \tag{3}$$

where, ρ_f is water density, p is pressure, $\vec{V}$ is the velocity, k_f is the water thermal conductivity, k_s is the silicon thermal conductivity, μ_f is the viscosity of the water, $c_{p,f}$ is specific heat of water, T is temperature.

For the solid, Eq. (3) can be written as:

$$k_s\nabla^2 T = 0, \tag{4}$$

with viscosity-temperature sensitivity as:

$$S_\mu = \mathrm{d}\mu/\mathrm{d}T, \tag{5}$$

and the viscous dissipation term as:

$$\phi = \mu def\vec{V}/(\mu def\vec{V}/2). \tag{6}$$

The viscosity is calculated by the parameters supplied by the NIST in the temperature range of liquid water, given as:

$$\mu = 0.11157 - 9.51523\times10^{-4}T + 2.7249\times10^{-6}T^2 - 2.61107\times10^{-9}T^3. \tag{7}$$

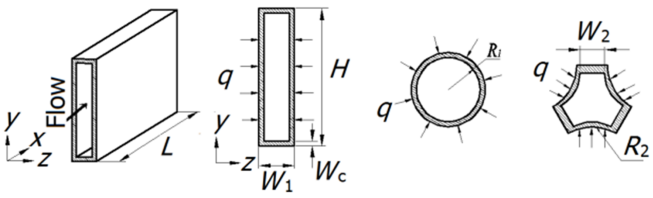

Fig. 2. Schematic diagram of computational domain.

The boundary conditions at the inlet, the outlet, the heating surface and the fluid-solid interface are given by Eqs. (8)–(11), respectively.

$$u = u_{\text{in}}, \nu = 0, w = 0, T = 293K, \tag{8}$$

$$P_{\text{f}} = P_{\text{out}}(1\text{atm}), \nu = 0, w = 0, \tag{9}$$

$$-k_s\partial T/\partial y = q_{\text{ou}}, \tag{10}$$

$$\begin{aligned} T_{s,\Gamma} &= T_{f,\Gamma}, \\ -k_s\frac{\partial T_s}{\partial n}\bigg|_\Gamma &= -k_f\frac{\partial T_f}{\partial n}\bigg|_\Gamma, \\ u|_\Gamma = 0,\ \nu|_\Gamma &= 0,\ w|_\Gamma = 0. \end{aligned} \tag{11}$$

The governing equations with boundary conditions were solved by the commercial CFD code, FLUENT. The equations were discretized by means of a fully implicit second order finite volume method with modified upwind advection scheme. The SIMPLE algorithm is used to resolve the pressure-velocity coupling. The numerical solution process is shown in Fig. 3.

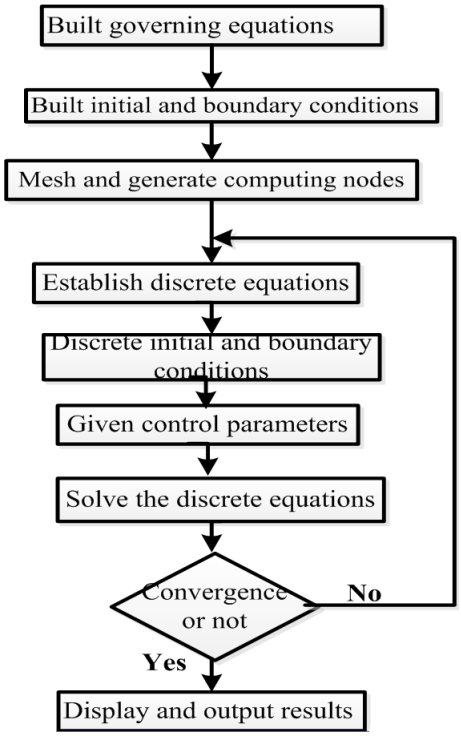

Fig. 3. The solution process.

IV. EXPERIMENTAL RESULTS

The experimental and simulation results for the fRe and heat transfer coefficient as a function of the Re number, are

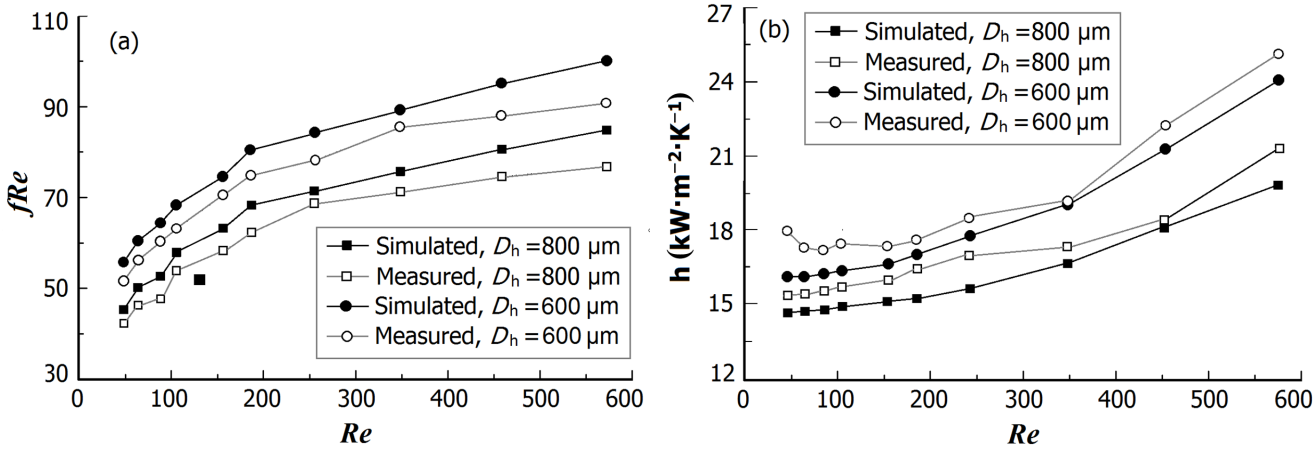

Fig. 4. Comparison of the experimental and simulation results for fRe (a), and heat transfer coefficient as a function of Re (b).

plotted in Fig. 4. The trends of experimental data and predicted curve are in good agreement over the entire range of Reynolds number being studied.

To compare with experimental data, the local thermal resistance is calculated using

$$R(x) = (T_{\max}(x) - T_{in})/q, \tag{12}$$

where, $R(x)$ and $T_{\max}(x)$ are thermal resistance and maximum temperature at x cm from the entrance, T_{in} is inlet water temperature, and q is heat flux at the heating area.

Validation of the numerical method was performed under uniform heat flux condition over the two side faces, as a benchmark case. Fig. 6 shows the thermal resistance data measured in this work and results by Tuckerman [9]. It can be seen that they agree well. The slight differences may be caused by different physical properties and outlet conditions. Apparently, the numerical method is appropriate for the present study.

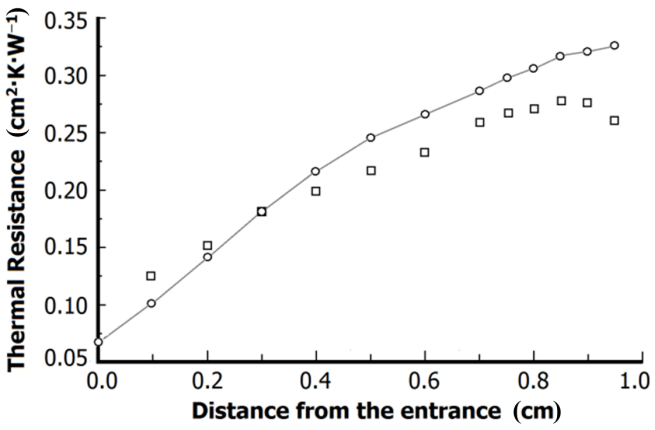

Fig. 5. Comparison of the measurement results (○) of thermal resistance with the data (□) by Tuckerman [9].

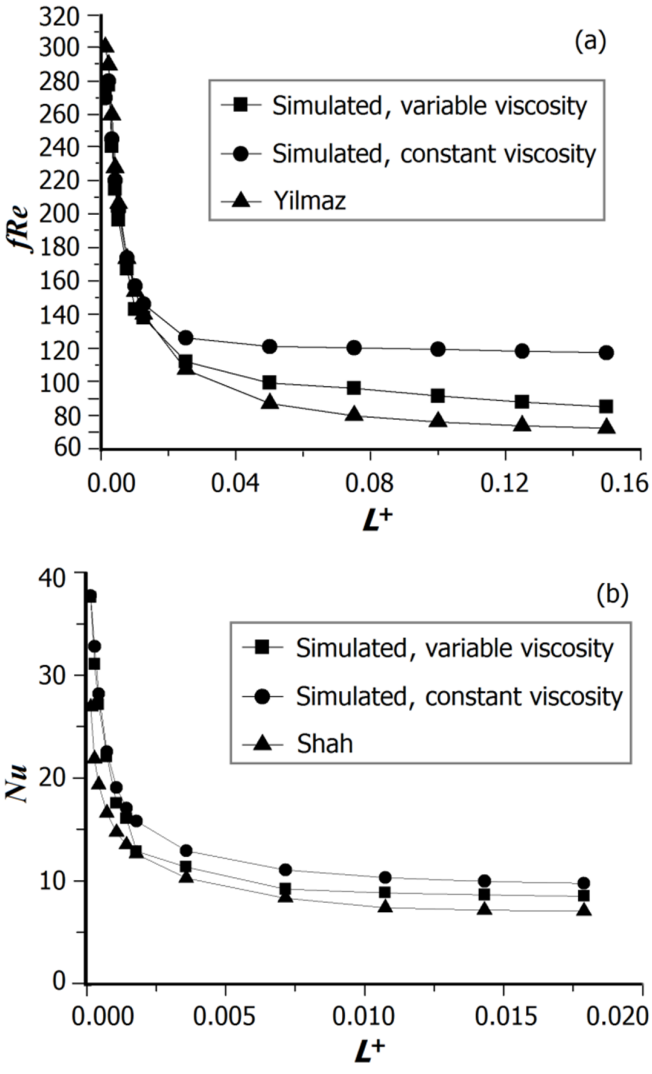

Fig. 6. The local fRe (a) and local Nusselt numbers (b) as a function of L^+.

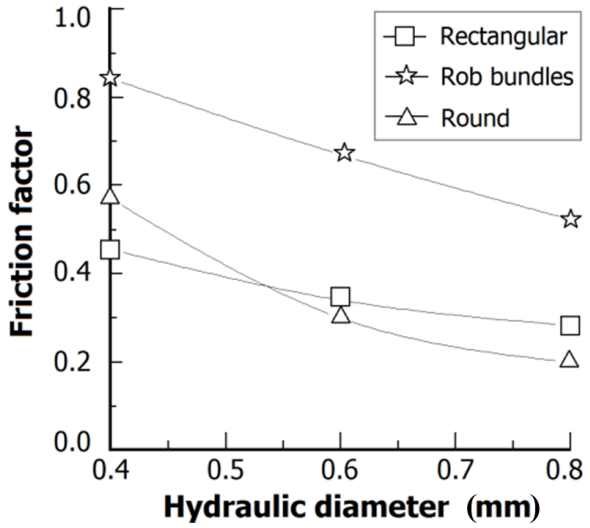

Fig. 7. Friction factor vs. hydraulic diameter for micro-channel of different shapes.

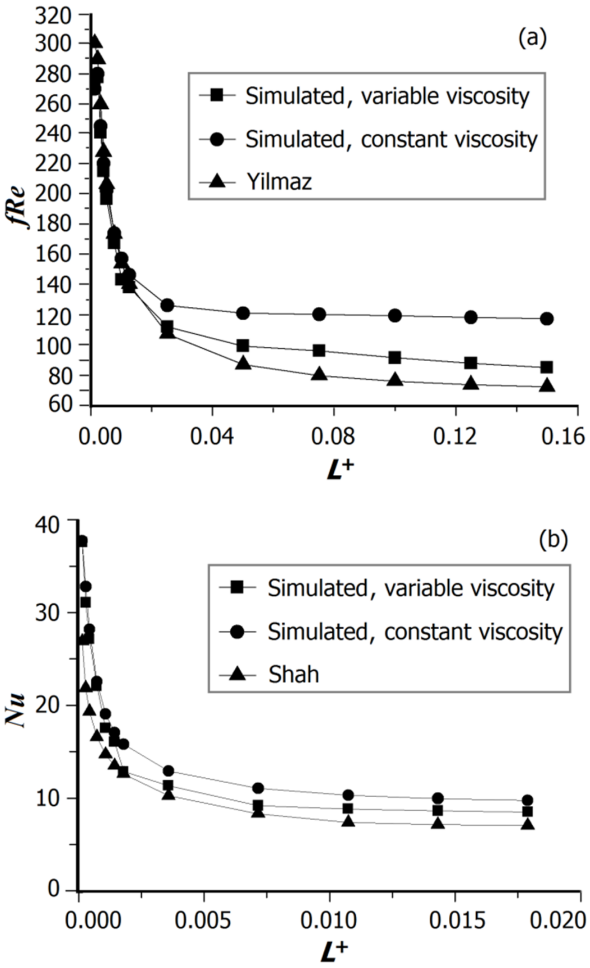

Fig. 8. Effects of heat flux uniformity on the fRe (a) and thermal efficiency of micro-channel of different shapes (b).

V. DISCUSSION

As shown in Fig. 6(a), the local fRe we simulated is in good agreement with analytical solution by Yilmaz [10]:

$$(fRe)_{\text{Yilmaz}} = \frac{13.76}{\sqrt{L^+}} + \frac{64\psi + K/L^+ - 13.76/\sqrt{L^+}}{1 + 0.98 \times 10^{-4} K^{3.14}/(L^+)^2}, \tag{13}$$

$$L^+ = L/(ReD_{\text{h}}). \tag{14}$$

The fRe reaches a constant value of about 120 when the hydrodynamic flow develops fully with a constant viscosity. However, the viscosity varies actually due to increasing water temperatures, and the fRe decreases continuously, as shown in Fig. 6(a). Therefore, the viscosity effect should be taken into account.

The calculated local Nusselt numbers agrees well with the theoretical results by Shah [11], too, as shown in Fig. 6(b). The data of variable viscosity are always less than the data of constant viscosity, as the viscous dissipation decreases heat

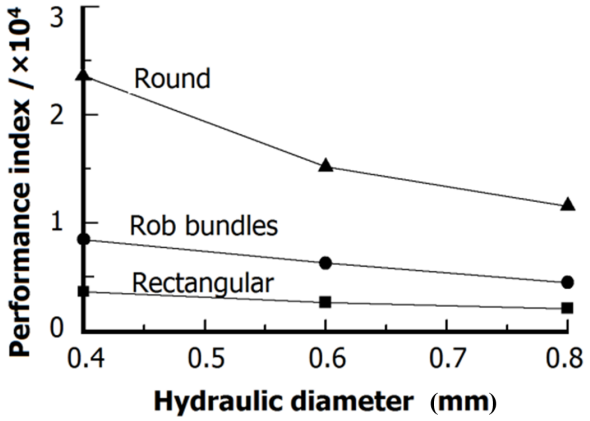

Fig. 9. Thermal efficiency vs. D_{h} for three types of micro-channels.

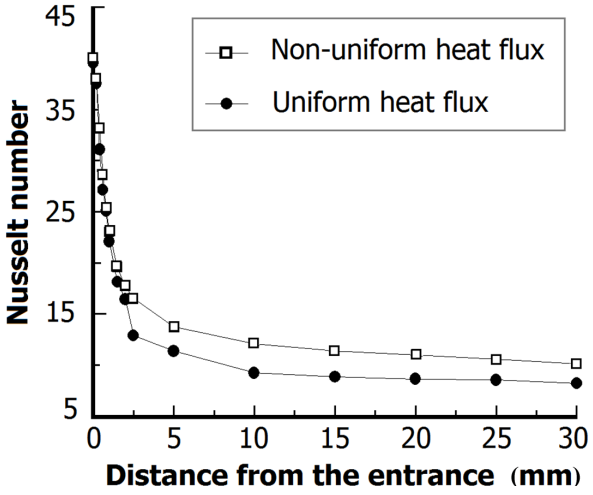

Fig. 10. Nusselt number as a function of D_{h} under uniform or non-uniform heating condition.

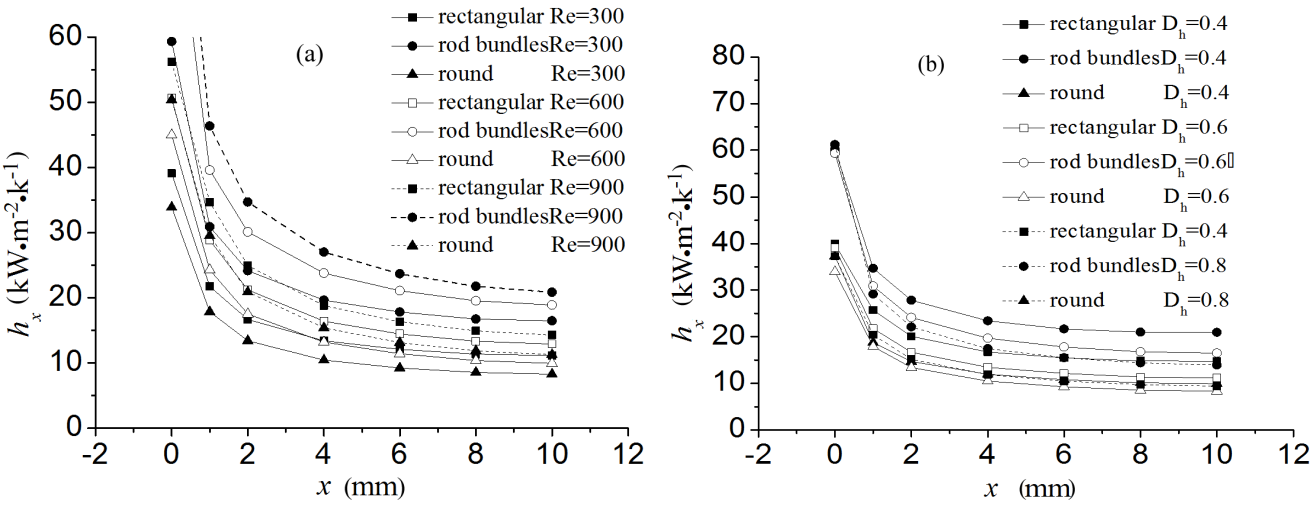

Fig. 11. Effect of Reynolds number (a) and hydraulic diameter (b) on heat transfer for the three types of micro-channels.

transfer efficiency. Differences in two sets of data disappear gradually with the flow development, as the viscous dissipation effects decrease.

The friction factors of laminar flows, as a function of hydraulic diameter, are shown in Fig. 7 for micro-channels in rectangular, round and rob bundle cross-sections. For the same cross-section, the friction factor decreases with increasing D_h. The rob bundle micro-channels have the highest friction factor, which causes the greatest energy dissipation. On the other hand, for $D_h = 0.6$–0.8 mm, the round micro-channels have the smallest friction factor.

Figure 8(a) shows that the fRe rises with Reynolds numbers under both uniform or non-uniform heat flux, but the fRe curve of non-uniform heating is always higher than that of the uniform heating, and the differences increase gradually with Re.

The performance index, defined as the ratio of heat transferred to total pumping power, is introduced for better understanding of the overall performance of the micro-channels,

$$\eta_{\text{eff}} = \frac{Q}{P_{\text{pump}}} = \frac{\rho_f c_p (T_{\text{out}}) - T_{\text{in}}}{\Delta p}. \quad (15)$$

Figure 8(b) shows the performance index, as a function of the Reynolds number, of differently shaped micro-channels of the same hydraulic diameter. Generally, the performance index decreases with increasing Reynolds number. This is due to the increased pressure drop which results in higher pumping power as the flow rate increases.

The performance index of different types of micro-channels with the same Reynolds numbers is illustrated in Fig. 9. The performance index decreases with increasing hydraulic diameter. Of all types of micro-channels, the round type has the highest performance index. The rod bundles type holds the second place.

Figure 10 shows the distributions of the Nusselt number (Nu) at different distances (x) from the entrance, under non-uniform or uniform heat flux at a specified Reynolds number. The Nusselt number of non-uniform flux is much higher than that of uniform heating condition at $5\,\text{mm} < x < 30\,\text{mm}$ due to the high heat flux in this region. The Nusselt number increases with the increase of heat flux.

As shown in Fig. 11(a), the heat transfer coefficient (h_x, in $\text{kW m}^{-2}\,\text{K}^{-1}$) increases with the Reynolds number at $D_h = 0.6\,\text{mm}$ for all the three types of micro-channels. The heat transfer enhancement contributes mainly to the thinner boundary layer at the higher Reynolds numbers. Fig. 11(b) shows the D_h effects on heat transfer coefficient at $Re = 300$. The heat transfer coefficient is greater at smaller hydraulic diameters, and it decreases along the flow direction of all the three types of cooling passages, as the flow becomes regular and the boundary layer thickens. The heat transfer coefficient is the highest at entrance region of the micro-channels, due to the entrance effect. Of the three types of micro-channels, the rod bundle type has the highest heat transfer coefficient, followed by rectangular type.

VI. CONCLUSION

The Navier-Stokes equations is still valid in the present study, and the variable viscosity effect should be taken into account. For our micro-channel configurations, the fRe increases almost linearly with the Re number. The heat transfer coefficient and thermal efficiency of micro-channels of the rod bundles is superior to the other channels.

[1] Yue J, Chen G, Yuan Q, *et al*. Chem Eng Sci, 2007, **62**: 2096–2108.

[2] Zhao T S and Bi Q C. Heat Mass Transfer, 2005, **48**: 3637–3647.

[3] Morini G L and Spiga M. Heat Transfer Eng, 2007, **129**: 308–318.
[4] Haddad O, Abuzaid M, Al-Nimr M. Entropy, 2005, **6**: 413–426.
[5] Khadrawi A F, Othman A, Al-Nimr M. Int J Thermophys, 2005, **26**: 905–914.
[6] Koo J and Kleinstreuer C. Heat Mass Transfer, 2004, **47**: 3159–3169.
[7] Judy J, Maynes D, Webb B W. Heat Mass Transfer, 2002, **45**: 3477–3489.
[8] Wu H Y and Cheng P. Heat Mass Transfer, 2003, **46**: 2519–2525.
[9] Tuckerman D B and Pease R F. Electron Devic Lett, 1981, **2** 126–129.
[10] Yilmaz T. J Enery Resour-ASME, 1990, **112**: 220–223.
[11] Shah R K and London A L. Laminar Flow Forced Convection in Ducts (Advances in Heat Transfer, Supplement 1). New York (USA): Academic Press, 1978.